文章编号：1001-9014(2024)01-0091-07

DOI:10.11972/j.issn.1001-9014.2024.01.013

Ultra-wideband absorption of C/Co composites achieved through metamaterial-based design

WANG Xiao-Kun, GUO Meng-Chao, LIANG Lei-Lei, LI Wei, TANG Dong-Ming, ZHANG Bao-Shan, YE Jian-Dong, YANG Yi*

(School of Electronic Science and Engineering, Nanjing University, Nanjing 210093, China)

Abstract: We synthesized C/Co composites via a facile one-step pyrolysis procedure and observed excellent dielectric dispersion properties at a 35 wt% filling concentration. At a thickness of 2.5 mm, the composites exhibited a minimum reflection of -23.7 dB at 11.2 GHz, with a bandwidth of 3.8 GHz (RL≤-10 dB). To further improve their absorption performance, we optimized the macrostructure of the absorber using an all-dielectric metamaterial design. The optimized design successfully extended the less than -10 dB absorption bandwidth to 15 GHz (7.0~22.0 GHz). Our results provide a useful reference for optimizing the preparation technology and structural design of high-performance microwave absorbers.

Key words: C/Co composites, microwave absorber, broadband absorption, metamaterial

基于超材料设计实现C/Co复合材料的超宽带吸收

王啸坤，过勐超，梁磊磊，李 威，唐东明，张豹山，叶建东，杨 燚*

（南京大学 电子科学与工程学院，江苏 南京 210093）

摘要：本文通过简单的一步热解法合成了C/Co复合材料，在材料质量填充浓度为35%时，观察到其具有优异的介电频散性能。当材料厚度2.5 mm时，该复合材料在11.2 GHz的最小反射率为-23.7 dB，小于-10 dB的带宽为3.8 GHz。为了进一步提高吸收体的吸波性能，利用全介质超材料的设计对吸收体的宏观结构进行优化，此方法成功地将小于-10 dB的吸收带宽扩展到15 GHz（7.0~22.0 GHz）。该研究结果可以为高性能微波吸收材料的制备工艺和结构设计提供有价值的参考。

关 键 词：C/Co化合物；微波吸收；宽带吸收；超材料

Introduction

In recent years, carbon-based absorbing materials such as carbon black, carbon nanotube, and graphene have gained significant attention due to their lightweight, dielectric dispersion, and loss characteristics. However, these pure carbon-based absorbers have some drawbacks, including single microwave loss mechanism, large thickness, and narrow bandwidth [1-4]. Fortunately, carbon-based magnetic metal composites have shown promise in overcoming these limitations by introducing a magnetic loss mechanism and enriching the regulatory mechanism, which alters the permittivity and permeability of the resulting composite materials [5-6].

Metal-organic frameworks (MOFs) are commonly used as generic precursors for preparing carbon-based composites. During the pyrolysis process, ferromagnetic metal nanoparticles in MOFs grow in situ and become embedded in the carbon material, enabling the regulation of complex permittivity and permeability by adjusting the compositions and structures of MOF-derived materials[7-10]. Previous studies have successfully produced lightweight absorbent materials, such as 3-D honeycomb-like FeCo/C nanocomposites, porous Co/C composites, and hierarchically porous Co/C composites, with excellent microwave absorption performance[11-13]. However, their practical application is still restricted by their narrow bandwidth and inadequate performance at low frequencies.

To address this issue, macrostructural design has

Received date: 2023-05-31, **revised date**: 2023-06-20　　**收稿日期**：2023-05-31，**修回日期**：2023-06-20

Foundation items: Supported by the National Natural Science Foundation of China (61271077, 11004095, 11104134).

Biography: Wang Xiao-Kun (1986-), male, Henan province, Doctor. Research area involves microwave absorption materials and techniques and microwave measurement technique. E-mail: absorber@aliyun.com

* **Corresponding author**: E-mail: malab@nju.edu.cn

been introduced to broaden the absorption bandwidth[14-18]. Recently, various carbon-based ADMMAs have been researched due to their own high dielectric loss and obvious dielectric dispersion, which is beneficial to broadband absorption [19-20]. Our group utilized a cylinder array structure design of all-dielectric metamaterial absorbers to broaden the absorption band. We achieved a less than -10 dB bandwidth from 6.1 to 18 GHz, with three absorption peaks, under a total thickness of 3.9 mm [21]. This method is expected to enhance the performance of carbon-based absorbing materials and broaden their absorption bandwidth.

In this work, we employed a simple and efficient one-step pyrolysis procedure to prepare MOF precursors based on a heat reaction of solvent at room temperature. C/Co composites with a rhombic dodecahedron shaped morphology were obtained by calcining the Co-based metal-organic frameworks at different temperatures. This environmentally friendly process is simpler compared to other methods that usually require high-temperature and high-pressure equipment. The effects of pyrolysis temperature, graphitization degree, and magnetic property were carefully investigated, and the resulting C/Co composites exhibited excellent absorbing performance. The minimum reflection achieved was -23.7 dB at 11.2 GHz with a thickness of 2.5 mm, and the bandwidth (RL≤-10dB) was 3.8 GHz. On this basis, we introduced all-dielectric metamaterial design to extend the bandwidth to 15 GHz, further improving the absorption performance.

1 Material and methods

1.1 Synthesis of C/Co composites

Initially, 5.284 g of 2-methylimidazole ($C_4H_6N_2$) and 1.164 g of cobaltous nitrate ($Co(NO_3)_2 \cdot 6H_2O$) were dissolved in 200 mL of deionized water and stirred for 2 h at room temperature. (Above chemical reagents were all of analytical grades, purchased from National Chemical Reagent Ltd., Shanghai, China). The resulting solution was then transferred into a 300 mL beaker and left to settle for 12 h at 60 °C. The resulting purple precipitate was collected by centrifugation, washed three times with deionized water and ethanol, and dried under vacuum conditions at 60 °C for 12 h. Next, the as-prepared Co-MOFs were annealed in an Ar atmosphere at 500 °C, 550 °C, and 600 °C for 2 hours, respectively, using a heating rate of 10 °C/min. The resulting samples were labeled as C/Co-500, C/Co-550, and C/Co-600, respectively. Finally, the C/Co-500, C/Co-550, and C/Co-600 were mixed with molten paraffin at a 35 wt% filling ratio for microwave measurements.

1.2 Characterization

The morphologies and microstructures of the C/Co composites were examined using transmission electron microscopy (TEM, JEOL JEM-2100) and scanning electron microscopy (SEM, Hitachi S4800) equipped with energy-dispersive X-ray spectrometry (EDS) for elemental analysis. The chemical composition of the C/Co composites was analyzed using X-ray photoelectron spectroscopy (XPS) on a PHI 5000 Versa Probe. The Raman spectra of the samples were obtained using a Renishaw inVia 2000 Raman spectrometer. The magnetic properties of the composites were evaluated using a vibrating sample magnetometer (VSM) at room temperature. The electromagnetic parameters of the samples were measured using the coaxial-line method with a vector network analyzer (VNA, Agilent PNA N5244A). Furthermore, the absorption properties of the C/Co metamaterial absorber under normal incidence were investigated through simulation using the electromagnetic simulation software CST Microwave Studio.

2 Results and discussion

The morphology of the C/Co composites is depicted in Fig. 1. SEM images of C/Co-500, C/Co-550, and C/Co-600 (Fig. 1a-c) reveal that the C/Co-500 sample does not form a rhombic dodecahedron, suggesting that the pyrolysis temperature at 500° C cannot facilitate the growth of C/Co particles, resulting in severe agglomeration of the composite. However, the C/Co-550 and C/Co-600 particles inherit the structure of the Co-MOF precursor, with radial sizes mostly in the range of 2~3 μm. The EDS spectrum (Fig. 1(d)) shows that the C/Co-550 particles are composed of C, Co, and O elements. The corresponding HRTEM images of the C/Co-550 sample (Fig. 1(e)-(g)) show that the particles have clear lattice fringes with a distance of 0.21 nm, which can be attributed to the typical Co (111) crystal planes[9, 22]. Additionally, a coating of amorphous carbon layers around metallic Co nanoparticles can be observed from Fig. 1g, which may provide good impedance matching characteristics for the C/Co composites[12].

Furthermore, we discuss the chemical state and composition of the C/Co composites, as determined by X-ray photoelectron spectroscopy (XPS). Fig. 2 (a) shows the XPS survey scan, which confirms the presence of C, Co, N, and O elements in the C/Co composites. The O element may be derived from water molecules in the air. Fig. 2(b) presents the C1s peak for all three samples, which can be divided into three binding energies corresponding to C-C (C-C/C=C), C-N, and C-O bonds, respectively. Notably, the C-C peak at 284.8 eV indicates that the carbon atoms in the C/Co particles are in the form of a sp^2 conjugated carbon skeleton[23], while the presence of C-N species suggests that nitrogen has been doped into the carbon skeleton, affecting the graphitization degree to some extent (Fig. 2 (e)). The N1s core survey spectrum (Fig. 2(d)) can be deconvoluted into three signals corresponding to pyridine N, pyrrole N, and graphitic N, respectively[24]. The creation of polar C-N bonds between C and N atoms may act as dipoles that respond to the polarization relaxation process under the electromagnetic field[25]. Additionally, N with extra valence electrons can serve as an electron donor and increase the conductivity of the carbon-based materials[26].

The high-resolution Co 2p spectrum of the three Co/C samples shows slight but significant differences (Fig. 2 (c)). The fitted spectra can be deconvoluted into two

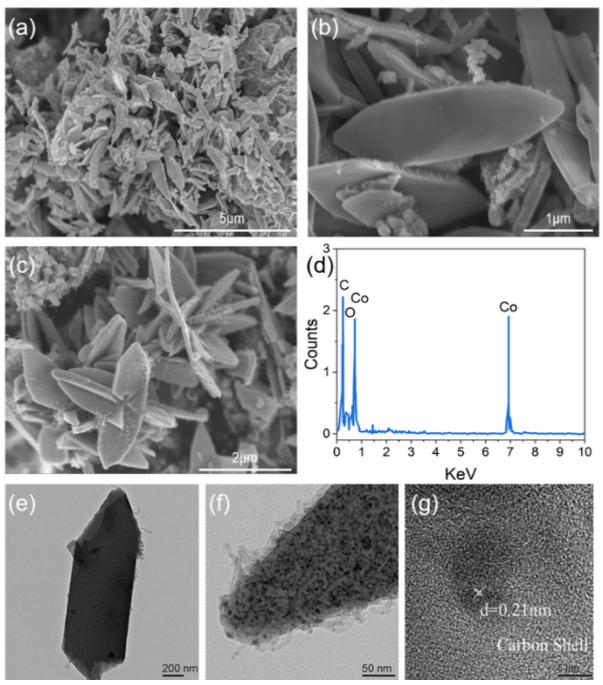

Fig. 1　SEM images of C/Co-500 (a), C/Co-550 (b) and C/Co-600 (c). EDS (d), TEM images (e, f) and HRTEM (g) of C/Co-550

图1　(a) C/Co-500, (b) C/Co-550, (c) C/Co-600样品的SEM图; C/Co-550样品的: (d) EDS能谱图, (e, f) TEM图, (g) HRTEM高分辨图

dominant peaks located at about 780.9 and 796.4 eV, corresponding to Co $2p_{3/2}$ and Co $2p_{1/2}$, respectively, which further confirms the metallic state of Co nanoparticles. Moreover, two shakeup satellite peaks at about 786.2 eV and 803.1 eV assigned to Co in the high valence state (Co^{2+} or Co^{3+}) are observed, indicating slight surface oxidation of Co nanoparticles. It is worth noting that the metallic Co can provide a magnetic response that improves the impedance matching characteristics and enhances the microwave absorption performance of the C/Co composites[13, 27].

The annealing temperature has a direct influence on the graphitization degree of the carbon layer, which in turn governs the dielectric properties. The graphitization degree can be evaluated by calculating the integrated intensity ratio of D and G peaks (I_D/I_G), where a larger value of I_D/I_G indicates a higher degree of lattice defect and lower graphitization degree of the carbon component. As depicted in Fig. 2(e), all the samples exhibit two prominent peaks at 1 340 cm^{-1} and 1 580 cm^{-1}, corresponding to the D band and G band, respectively. The I_D/I_G values of C/Co-500, C/Co-550, and C/Co-600 are 0.92, 0.90, and 0.89, respectively. The ratio decreases with annealing temperature, and the ratio of C/Co-550 is almost equal to C/Co-600. These findings suggest that the C/Co-550 and C/Co-600 have high graphitization degree, which is in favor of conduction loss[28-29].

The magnetic hysteresis loops of C/Co samples obtained at different pyrolysis temperatures are shown in Fig. 2(f). Specifically, the saturation magnetization (Ms) values of samples C/Co-500, C/Co-550, and C/Co-600 are 18.2, 70.4, and 26.7 emu·g^{-1}, respectively. Additionally, the coercivity (Hc) of C/Co-500, C/Co-550, and C/Co-600 is 139.3, 134.1, and 141.2 Oe, respectively. All C/Co composites exhibit typical ferromagnetic hysteresis loops. Notably, the Ms values of C/Co-500 and C/Co-600 are significantly lower than that of C/Co-550, which could be attributed to the crystalline degree of metallic Co nanoparticles.

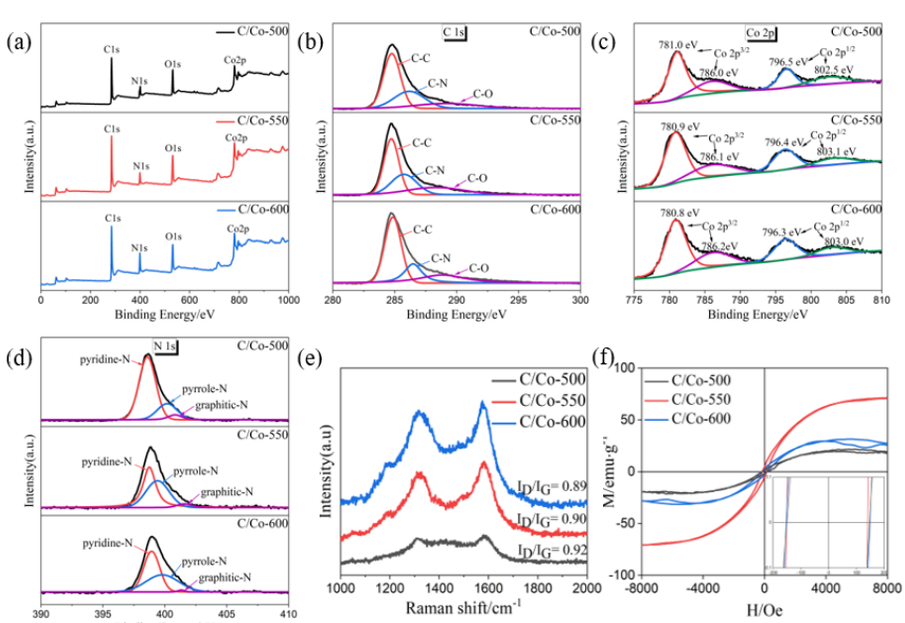

Fig. 2　XPS spectra of: (a) survey spectrum; (b) C 1s; (c) Co 2p; (d) N 1s; (e) Raman and (f) Magnetic hysteresis loops of C/Co-500, C/Co-550 and C/Co-600

图2　C/Co-500, C/Co-550, C/Co-600样品: (a) XPS测试光谱图; (b) 高分辨C 1s光谱图; (c) 高分辨Co 2p光谱图; (d) 高分辨N 1s光谱图; (e) Raman光谱图; (f) 磁滞回线图

The storage and attenuation energy capacity of a material is represented by the real and imaginary parts of its complex permittivity (ε', ε'') and complex permeability (μ', μ''), respectively. Figure 3(a) illustrates the real and imaginary parts of the complex permittivity for C/Co-500, C/Co-550, and C/Co-600. The values of ε' for all three samples decrease with increasing frequency, with the ε' and ε'' values of C/Co-500 being significantly lower than those of C/Co-550 and C/Co-600. This can be attributed to the lower graphitization degree of the carbon component and the incomplete reduction of the Co element in C/Co-500. In other words, the low pyrolysis temperature (500 °C) cannot form a mosaic structure of C and Co. The dielectric response of C/Co composites is mainly influenced by the interface effect between the metal and carbon. The interaction between π and d orbitals of the metal and carbon leads to orbital hybridization, resulting in various physical properties. Additionally, conduction loss also contributes to the dielectric response. Furthermore, the interface polarization effect of the C/Co-500 sample is weaker than that of the other two samples due to the structural features of MOF-derived metal/carbon composites, resulting in the lowest values of ε' and ε''. Although the initial real permittivity of C/Co-550 and C/Co-600 is similar, the C/Co-550 sample exhibits the most pronounced change in ε' with increasing frequency due to its moderate graphitization degree compared to the C/Co-600 sample, thus demonstrating better dispersion characteristics.

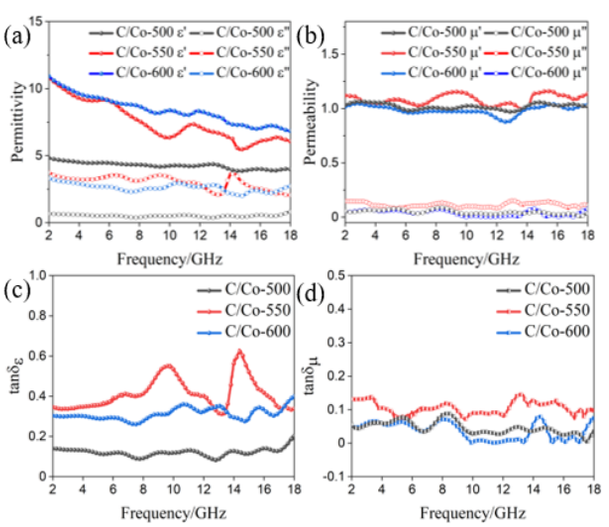

Fig. 3 Complex permittivity: (a) and complex permeability; (b) of C/Co-500, C/Co-550 and C/Co-600 composites with 35 wt% filling concentration; (c) dielectric loss tangent; (d) magnetic loss tangent of C/Co-500, C/Co-550 and C/Co-600 composites
图3 质量填充浓度为35%的C/Co-500, C/Co-550, C/Co-600复合材料: (a) 复介电常数; (b)复磁导率; (c) 介电损耗正切, (d) 磁损耗正切

Fig. 3(b) shows that the μ' and μ'' values of the three samples are very close and low in the whole frequency band. The C/Co-550 has the highest μ' and μ'' values, consistent with the static magnetic parameters (Fig. 2(a)). However, the maximum μ' and μ'' values of C/Co-550 are only 1.08 and 0.10, respectively, indicating that the magnetic loss of C/Co composites contributes relatively little to the attenuation of electromagnetic waves. Fig. 3(c) and 3(d) reveal that the dielectric loss angle ($\tan\delta_\varepsilon$) is much larger than the magnetic loss angle ($\tan\delta_\mu$). Based on the above analysis, it can be concluded that the dominant factor in the attenuation of electromagnetic waves in C/Co composites is dielectric loss.

Dielectric loss mechanisms are often described by the Cole-Cole model, where the semicircle in the Cole-Cole curve corresponds to polarization loss, while the linear part indicates conductivity loss. In Fig. 4(a), the Cole-Cole curves of C/Co-500, C/Co-550, and C/Co-600 are plotted according to Eq. (1) and Eq. (2)[29]:

$$\varepsilon' = \varepsilon_\infty + \frac{\varepsilon_s - \varepsilon_\infty}{1+\omega^2\tau^2},\ \varepsilon'' = \frac{(\varepsilon_s - \varepsilon_\infty)\omega\tau}{1+\omega^2\tau^2} \quad (1)$$

$$\left[\varepsilon' - \frac{1}{2}(\varepsilon_s + \varepsilon_\infty)\right]^2 + (\varepsilon'')^2 = \left[\frac{1}{2}(\varepsilon_s + \varepsilon_\infty)\right]^2, \quad (2)$$

where ε_s is the static permittivity, $\varepsilon_\infty$is the permittivity at ultra-high limit frequency, and ω is the alternating electric field frequency, τ is the relaxation time. Multiple semicircles can be observed in the Cole-Cole curves of all three samples, indicating that the interfacial polarization effect plays an essential role in the dielectric loss of C/Co composites. Notably, the effect is most prominent in the C/Co-550 sample, owing to its higher dielectric loss capacity compared to C/Co-500 and C/Co-600.

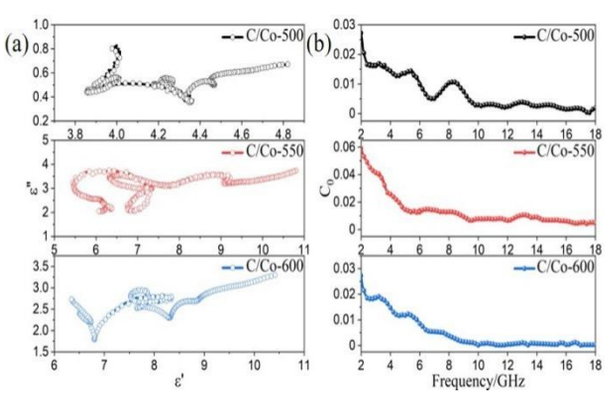

Fig. 4 Cole-Cole circles: (a) and C_0 curves; (b) of C/Co-500, C/Co-550 and C/Co-600
图4 C/Co-500, C/Co-550, C/Co-600样品: (a) Cole-Cole圆图; (b) Co曲线

The main sources of magnetic loss include domain wall resonance, natural resonance, and eddy current loss. However, in the C/Co composite, the Co nanoparticles are below the critical size for a single domain, which means there is no domain wall resonance. Moreover, the term C_0, as defined in Eq. (3), is commonly used to represent eddy current loss[30]. When the magnetic loss is solely caused by eddy current loss, the C_0 value remains constant regardless of the frequency. From Fig. 4(b), it is evident that as the frequency increases, the C_0 values tend to converge to a constant, indicating that magnetic

loss primarily arises from the eddy current effect in the high-frequency range. Thus, at low frequencies, magnetic loss is dominated by natural resonance, while at high frequencies, it is primarily attributed to eddy current loss[17].

$$C_0 = \mu''(\mu')^{-2} f^{-1}. \tag{3}$$

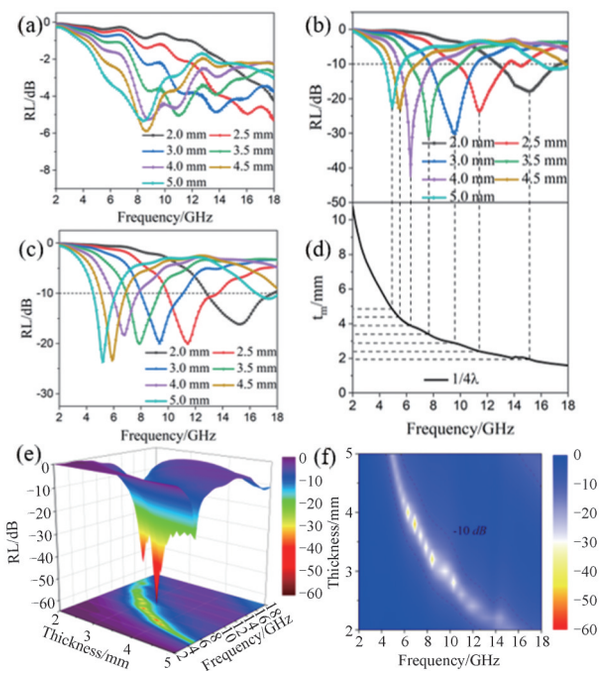

Fig. 5　RL curves of C/Co-500 (a), C/Co-550 (b) and C/Co-600 (c), (d) t_m curve; (e) three-dimensional representations and (f) two-dimensional color contour RL values of C/Co-550
图 5　(a) C/Co-500; (b) C/Co-550; (c) C/Co-600 样品的反射损耗曲线, C/Co-500 样品的 (d) tm 曲线; (e) 三维反射损耗示意图; (f) 二维等值线反射损耗示意图

To evaluate the microwave absorption performance of a single-layer absorber, the reflection loss (RL) values can be calculated using transmission line theory. The equations used to calculate these values are shown in Eq. (4) and Eq. (5):

$$\mathrm{RL(dB)} = 20\log\left|\frac{z_{in}-1}{z_{in}+1}\right|, \tag{4}$$

$$z_{in} = \sqrt{\frac{\mu_r}{\varepsilon_r}}\tan h\left[\mathrm{j}\frac{2\pi fd}{c}\sqrt{\varepsilon_r\mu_r}\right], \tag{5}$$

where z_{in} is the normalized input impedance, f is the frequency, and d is the layer thickness. Figures 5(a)-(c) display the RL values of three C/Co composites with different layer thicknesses across the 2~18 GHz frequency range. Black lines indicate areas with RL values lower than -10 dB. The results reveal that the C/Co-500 sample has poor microwave absorption ability, as its RL value does not reach -10 dB within the tested frequency range. In contrast, the C/Co-550 and C/Co-600 samples exhibit excellent broadband absorbing performance in both C and X bands. Notably, Fig. 5(b)-(f) illustrates that C/Co-550 achieves a minimum RL of about -42.5 dB at 6.3 GHz and 4 mm thickness, while at 2.5 mm thickness, it shows an effective absorption bandwidth of 3.8 GHz with a minimum RL value of -23.7 dB.

In the case of absorbing materials, the absorption peak can be explained by the λ/4 resonance model. The ideal matching thickness for the absorbing coating should be an odd mutiple of 1/4 wavelength, which can be calculated using the following formula[17]:

$$t_m = \frac{nc}{4f_m\sqrt{|\mu_r\varepsilon_r|}} \quad (n = 1,3,5\cdots), \tag{6}$$

where c is the light velocity in vacuum, f_m is the peak frequency of absorbing materials. Fig. 5(b), (d) shows the simulation results of the matching thickness (t_m) for the C/Co-550 sample under λ/4 conditions. According to Eq. (6), the matching thickness is inversely proportional to the frequency. If μ' and ε' are constants, the optimal matching thickness will decrease as the frequency increases. However, this leads to a lack of change in the electrical thickness of the coating, resulting in a deterioration in the absorbing performance. Conversely, if the value of μ' or ε' decreases with increasing frequency while maintaining the coating thickness at λ/4, it becomes possible to achieve an ideal matching condition. This demonstrates that frequency dispersion of the material can significantly enhance the absorbing performance.

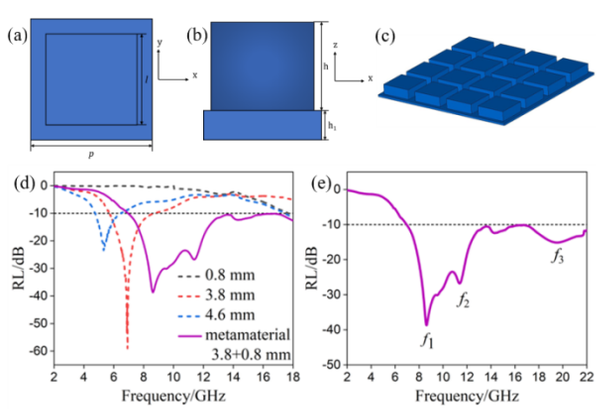

Fig. 6　Structure of one unit: (a) top view; (b) cross section view; (c) periodic unit structures; (d) Reflection loss of single layer and all-dielectric metamaterial of C/Co-500 composite; (e) Reflection loss of C/Co-500 all-dielectric metamaterial absorbers under 2~22 GHz
图 6　平板-方块型周期单元: (a)俯视图; (b)侧面图; (c)周期单元结构图; (d)单层 C/Co-500 复合材料和全介质型 C/Co-500 超材料吸收体的反射损耗; (e)全介质型 C/Co-500 超材料吸收体在 2~22 GHz 的反射损耗

The C/Co-550 sample exhibits good absorbing performance and bandwidth, but it has some limitations such as the thick matching thickness, the narrow absorbing bandwidth, and strong dependency on λ/4 resonance to acquire absorption peaks. To address these issues, a periodic unit structure of C/Co-550 metamaterial absorber is proposed, which can introduce multiple response mechanisms to enhance the absorbing performance. The designed periodic unit structure is shown in Fig. 6(a)-(c), with a periodic boundary condition used in both x and y directions and an open boundary applied in the z di-

rection. The geometric parameters are determined as h= 3.8 mm, h_1=0.8 mm, l=11 mm, and p=14 mm. The simulated RL curve for the metamaterial absorber with a 35 wt% C/Co-550 filling concentration is plotted in Fig. 6 (d)-(e), which shows that the absorption bandwidth (RL ≤-10 dB) reaches up to 15.0 GHz (7.0~22.0 GHz), covering the whole X, Ku band and most of C band, and there are three absorption peaks appear near 8.6 GHz (f_1), 11.4 GHz (f_2) and 19.5 GHz (f_3), respectively. In contrast, the absorption bandwidth of the single layer C/Co 550 coating with the same thickness is only 1.7 GHz (4.8-6.5 GHz). Clearly, the periodic metamaterial structure greatly broadens the absorption bandwidth, which is 8.8 times more than the single-layer C/Co-550 coating at the same thickness. Moreover, the areal density of the C/Co-550 plate-block metamaterial with a thickness of 4.6 mm is only 3.8 kg·m^{-2}, lower than that of the single C/Co-550 coating (5.38 kg·m^{-2}). Thus, the periodic unit structure of the metamaterial absorber has great advantages in terms of absorption bandwidth and areal density compared with the single-layer coating.

Fig. 7 depicts the distribution of magnetic field density, electric field density, and power loss density at three absorption peaks (f_{1-3}), revealing the absorption mechanisms of the C/Co-550 metamaterial absorber. At the f_1 peak, as displayed in Fig. 7(a)-(c), the magnetic field density mainly resides at the bottom of the periodic element, while the electric field density is distributed at the top of the element and the gap between the elements. The phase difference close to π/2 indicates the formation of standing waves inside the element. By comparing the distribution of power loss density (Fig. 7(c)) and the RL curve of the single-layer C/Co-550 coating in Fig. 6 (d), the absorption at 8.6 GHz is confirmed to be mainly caused by the λ/4 resonance inside the structural unit.

Regarding the mechanism of the peak (f_2), Fig. 7 (d)-(f) illustrates that the magnetic field density is distributed in the gap of periodic units and the bottom of the groove, while Fig. 7(e) shows the electric field density to be distributed at the edge of the cavity between the adjacent units. The power loss density mainly occurs on both sides of the unit, especially at the top corner, indicating that the absorption peak at 11.4 GHz is due to the edge diffraction effect and the resonance occurring between the periodic structure units[31].

Fig. 7(g),(h) reveals that the electric and magnetic fields at 19.5 GHz have two concentration regions within the unit. Fig. 7(i) displays the power loss density at the top and bottom plates of the periodic structure, which is close to the λ/4 and 3λ/4 interference region, indicating that the absorption peak (f_3) is caused by multiple λ/4 resonance. Considering the EM parameters shown in Fig. 4(a),(b), the dielectric loss of C/Co-550 is significantly higher than the magnetic loss at such a high frequency, and the position of the power loss density is similar to the area of the electric field density. Overall, the C/Co-550 sample demonstrates excellent loss capability for the periodic structure units, while the metamaterial absorber also enhances the microwave absorption performance and broadens the absorption bandwidth[32-33].

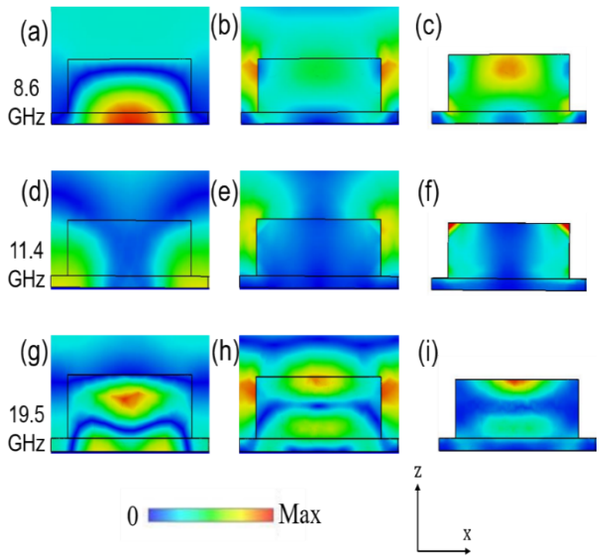

Fig. 7 The distributions of magnetic field density, electric field density and power loss density under normal incidence at 8.6 GHz (a, b, c), 11.4 GHz (d, e, f) and 19.5 GHz (g, h, i)
图7 C/Co-550平板-方块型超材料吸收体单个结构单元在8.6 GHz处的:(a)磁场强度分布图;(b)电场强度分布图;(c)能量损耗分布图;在11.4 GHz处的;(d) 磁场强度分布图;(e)电场强度分布图;(f)能量损耗分布图;在19.5 GHz处的;(g)磁场强度分布图;(h)电场强度分布图,(i)能量损耗分布图

3 Conclusions

In conclusion, we have successfully prepared MOF-derived C/Co composites with a rhombic dodecahedron shaped structure using a simple and cost-effective one-step procedure. The C/Co composite absorbents exhibited excellent dielectric dispersion properties at a filling concentration of 35 wt%. With a thickness of 2.5 mm, the minimum reflection reached -23.7 dB at 11.2 GHz, and the bandwidth (RL≤-10 dB) covered 3.8 GHz. Moreover, by combining traditional absorbing materials with all-dielectric metamaterial design, we achieved a remarkable absorption bandwidth (RL≤-10 dB) of 15.0 GHz at 4.8 mm, thanks to the periodic structures employed. These findings have significant implications for the development and optimization of super broadband microwave absorbers. Our work provides valuable insights and serves as a reference for future research in this field.

References

[1] Novoselov K S, Geim A K, Morozov S V, *et al*. Electric Field Effect in Atomically Thin Carbon Films [J]. *Science*, 2004, **306**(5696): 666-669.
[2] Asbeck P, Kangmu L, Jeong-Sun M. Graphene: Status and Prospects as a Microwave Material [C]//Wireless and Microwave Technology Conference.IEEE, 2011
[3] Vazquez E., Prato M. Carbon nanotubes and microwaves: Interactions, responses, and applications [J]. *ACS Nano*, 2009, **3** (12): 3819-3824.
[4] Sun H, Che R, You X, *et al*. Cross-stacking aligned carbon-nanotube films to tune microwave absorption frequencies and increase absorption intensities [J]. *Advanced Materials*, 2014, **26**(48): 8120-

8125.
[5] Qing Y, Min D, Zhou Y, *et al*. Graphene nanosheet-and flake carbonyl iron particle-filled epoxy-silicone composites as thin-thickness and wide-bandwidth microwave absorber[J]. *Carbon*, 2015, **86**: 98-107.
[6] Quan B, Liang X, Ji G, *et al*. Strong electromagnetic wave response derived from the construction of dielectric/magnetic media heterostructure and multiple interfaces[J]. *ACS Applied Materials & Interfaces*, 2017, **9**(11): 9964-9974.
[7] Zhang Z, Cai Z, Wang Z, *et al*. A review on metal-organic framework-derived porous carbon-based novel microwave absorption materials[J]. *Nano-Micro Letters*, 2021, **13**(1): 56.
[8] Shu J, Cao W, Cao M. Diverse metal-organic framework architectures for electromagnetic absorbers and shielding[J]. *Advanced Functional Materials*, 2021, **31**(23): 2100470.
[9] Ma H, Du X, Wu C, *et al*. Co/C broad band electromagnetic wave absorption composite derived from preferred precursor ZIF-67: preparation and performance [J]. *Journal of Materials Science Materials in Electronics*, 2020, **31**: 6418-6434.
[10] Shu R, Wu Y, Li X, *et al*. Fabrication of yolk-shell NiCo alloy@C composites derived from trimetallic metal-organic frameworks as light-weight and high-performance electromagnetic wave absorbers [J]. *Composites Part A: Applied Science and Manufacturing*, 2021, **147**:106451.
[11] Li D, Liang X, Liu W, *et al*. Adjustable 3-D structure with enhanced interfaces and junctions towards microwave response using FeCo/C core-shell nanocomposites[J]. *Journal of Colloid and Interface Science*, 2017, **507**: 131-138.
[12] Qiang R, Du Y, Chen D, *et al*. Electromagnetic functionalized Co/C composites by in situ pyrolysis of metal-organic frameworks(Zif-67) [J]. *Journal of Alloys and Compounds*, 2016, **681**: 384-393.
[13] Wang L, Bai X, Wen B, *et al*. Honeycomb-like Co/C composites derived from hierarchically nanoporous Zif-67 as a lightweight and highly efficient microwave absorber[J]. *Composites Part B-Engineering*, 2019, **166**: 464-471.
[14] Huang Y, Song W L, Wang C, *et al*. Multi-scale design of electromagnetic composite metamaterials for broadband microwave absorption[J]. *Composites Science and Technology*, 2018, **162**: 206-214.
[15] Huang Y, Yuan X, Chen M, *et al*. Ultrathin flexible carbon fiber reinforced hierarchical metastructure for broadband microwave absorption with nano lossy composite and multi-scale optimization[J]. *ACS Applied Materials&Interfaces*, 2018, **51**(10): 44731-44740.
[16] Zhang N, Gu W, Zhao Y, *et al*. The enhanced microwave broadband absorbing ability of carbon microspheres via electromagnetic simulating honeycomb design [J]. *Journal of Materials Science: Materials in Electronics*, 2020, **32**: 25809-25819.
[17] Tan R, Zhou F, Chen P, *et al*. PANI/FeCo@C composite microspheres with broadband microwave absorption performance [J]. *Composites Science and Technology*, 2022, **218**: 109143.
[18] Zhang N, Han M, Wang G, *et al*. Achieving broad absorption bandwidth of the Co/carbon absorbers through the high-frequency structure simulator electromagnetic simulation [J]. *Journal of Alloys and Compounds*, 2021, **883**: 160918.
[19] Guo M, Wang X, Zhuang H, *et al*. Characteristics of high-contrast gratings based spoof surface plasmon polaritons and the application in microwave all-dielectric metamaterial absorbers[J]. *Journal of Applied Physics*, 2022, **131**:063103
[20] Guo M, Wang X, Zhuang H, *et al*. 3D printed low-permittivity all-dielectric metamaterial for dual-band microwave absorption based on surface lattice resonances [J]. *Physica Scripta*, 2022, **97**: 075504.
[21] Guo M, Wang X, Zhuang H, *et al*. Broadband carbon-based all-dielectric metamaterial absorber enhanced by high-contrast gratings based spoof surface plasmon polaritons [J]. *Physica Scripta*, 2023, **98**: 035518.
[22] Wang Y, Di X, Gao X, *et al*. Rational construction of Co@C polyhedrons covalently-grafted on magnetic graphene as a superior microwave absorber[J]. *Journal of Alloys and Compounds*, 2020, **843**: 156031.
[23] Liang L, Liu Z, Xie L, *et al*. Bamboo-like N-doped carbon tubes encapsulated coni nanospheres towards efficient and anticorrosive microwave absorbents[J]. *Carbon*, 2021, **171**: 142-153.
[24] Zhang X, Zhang X, Yuan H, *et al*. CoNi nanoparticles encapsulated by nitrogen-doped carbon nanotube arrays on reduced graphene oxide sheets for electromagnetic wave absorption[J]. *Chemical Engineering Journal*, 2020, **383**: 123208.
[25] Wang J, Ciucci F. Boosting bifunctional oxygen electrolysis for N-doped carbon via bimetal addition [J]. *Small*, 2017, **13**(16): 1604103.
[26] Liu P, Zhang Y, Yan J, *et al*. Synthesis of lightweight N-doped graphene foams with open reticular structure for high-efficiency electromagnetic wave absorption[J]. *Chemical Engineering Journal*, 2019, **368**: 285-298.
[27] Meng X, Dong S. Design and construction of lightweight C/Co heterojunction nanofibres for enhanced microwave absorption performance [J]. *Journal of Alloys and Compounds*, 2019, **810**: 151806.
[28] Xu H, Zhang Z, Xu W. Influence of graphitization degree of PAN based CF on its resistivity[J]. *New Chemical Materials*, 2021, **49**(2): 158-160,164.
[29] Liang X, Wang G, Gu W, *et al*. Prussian blue analogue derived carbon-based composites toward lightweight microwave absorption [J]. *Carbon*, 2021, **177**: 97-106.
[30] Chen J, Zheng J, Huang Q, *et al*. Carbon fibers@Co-ZIFs derivations composites as highly efficient electromagnetic wave absorbers [J]. *Journal of Materials Science and Technology -Shenyang-*, *2021*, 94: 239-246.
[31] Guo M, Wang X, Zhuang H, *et al*. Characteristics of high-contrast gratings based spoof surface plasmon polaritons and the application in microwave all-dielectric metamaterial absorbers[J]. *Journal of Applied Physics*, 2022, **131**(6): 063103.
[32] Li W, Wu T, Wang W, *et al*. Broadband patterned magnetic microwave absorber [J]. *Journal of Applied Physics*, 2014, **116**(4): 044110.
[33] Zhuang H, Wang X, Wang J, *et al*. Broadband microwave metamaterial absorber based on magnetic periodic elements [J]. *Journal of Physics D: Applied Physics*, 2020, **53**(25): 255502.